Molecular Catalysis 530 (2022) 112489

Contents lists available at ScienceDirect

Molecular Catalysis

journal homepage: www.journals.elsevier.com/molecular-catalysis

The water assisted vinylene mechanism for cobalt Fischer-Tropsch synthesis assessed by multi-catalyst modelling of kinetics and deactivation

Erling Rytter *, Anders Runningen [1], Edd Blekkan, Magne Hillestad

Department of Chemical Engineering, Norwegian University of Science and Technology (NTNU), Sem Sæland vei 4, NO-7491, Trondheim, Norway

ARTICLE INFO

Keywords:
Fischer-Tropsch
Kinetics
Deactivation
Mechanism
Cobalt catalyst

ABSTRACT

The paper describes development of a mechanism and a consistent rate expression for Fischer-Tropsch (FT) synthesis over cobalt-based catalysts. The developed mechanism relies on a two-step hydrogen assisted activation of CO. The carbon atom of CO is first hydrogenated by surface hydrogen to formyl; followed by the rate-limiting step whereby the oxygen atom is hydrogenated by adsorbed water. The produced CH* monomer is incorporated into the growing chain giving vinylene intermediate. The vinylene intermediate is either terminated to an olefin by adding hydrogen to the α-carbon atom or propagates by adding hydrogen to the β-carbon position. The resulting expression for CO consumption, the Fischer-Tropsch rate, can respond positively or negatively to the partial pressure of water, in agreement with experimental observations. A special feature is that the chain propagation probability does not depend on the partial pressure of hydrogen. The resulting kinetic model is tested on several cobalt catalysts supported on alumina; spanning from γ-alumina with average pore sizes ranging from 6.1 to 18.3 nm to α-alumina with a wide pore structure; and with cobalt particle sizes from 8 to 19 nm. Water was added sequentially to the syngas feed, causing enhanced deactivation, for testing the water response on activity and selectivity. A deactivation model comprising sintering and cobalt oxidation, and the FT-kinetics, describe the observed CO conversions with great precision for all catalysts. Selectivities are also well described, but with slight deviations at least partly due the effect of deactivation. Trends in some of the kinetic parameters are rationalized in terms of cobalt crystallite and pore sizes.

1. Introduction

The overall reaction in low-temperature Fischer-Tropsch synthesis (FTS) from synthesis gas (syngas) can be described as

$$n\ CO + 2n\ H_2 \rightarrow C_nH_{2n} + n\ H_2O \quad (1)$$

assuming a general chain length and the primary product to be an olefin. Stoichiometric amount of water is produced for each carbon atom in the product. In a recent series of papers on cobalt catalyzed FTS we have demonstrated that water is not a silent spectator but plays a significant role in all parts of FTS [1–3]. Type and structure of the support is an important parameter in developing an FT-catalyst system. Frequently used support materials are alumina, silica and titania [4]; they behave differently when cobalt is deposited. Furthermore, there are huge differences in properties within each class of support that result in variations in activity and polymerization probability, e.g., as detected by the C_{5+} selectivity [5–8]. Without exception, for all catalyst systems and process conditions, water added to the syngas feed and water produced during FT synthesis, improve selectivity to higher hydrocarbons. It follows that the C_{5+} selectivity increases with CO conversion due to positive effect of indigenously produced water.

Krishnamoorthy et al. investigated cobalt supported on silica and found that both C_{5+} selectivity and CO activation rate increase by adding water to the feed [9]. Correlations were found by adding water during FTS for more than ten different γ-alumina supported cobalt FT catalysts, with large variations in pore sizes [3]. It was shown that due to positive correlation between pore size and cobalt crystallite size, there is a concurrent increase in C_{5+} with pore diameter. This increase in selectivity was found to be due to higher Anderson-Schultz-Flory chain propagation probabilities; α [10]. High α values were ascribed to larger cobalt crystallites that promote CO activation with consequently higher surface coverage of CH_x polymerization monomers. Increase in cobalt crystallite size with increasing pore diameter was also detected when using silica supports [11]. Importantly, close correlation was found

* Corresponding author.
E-mail address: rytter@ntnu.no (E. Rytter).
[1] Present address: Citec Norway AS, Strandveien 37, 1366 Lysaker; anders.runningen@citec.com

https://doi.org/10.1016/j.mcat.2022.112489
Received 8 April 2022; Received in revised form 30 June 2022; Accepted 1 July 2022
Available online 29 August 2022

between positive responses to water for C_{5+} selectivity and CO conversion [3], pointing at the same mechanistic origin. Analyses showed that added water imposes a significantly enhanced probability for chain initiation *vs.* termination to methane. This was attributed to higher relative cobalt surface coverage of water or hydroxyl and CH_x monomers relative to hydrogen. Visconti and co-workers tested a Co on γ-alumina catalyst in extended runs with added water [12]. Their results comply with the observations above, and they interpreted the data in terms of water suppressing hydrogen activity.

Several mechanisms for activation of CO and insertion into the growing chain have been scrutinized. This comprises the carbide mechanism or unassisted CO dissociation [13–18] hydrogen assisted CO dissociation [19,20], direct CO insertion [21–23], and the enol mechanism [24]. The latter two mechanisms appear more relevant for iron catalysts and formation of oxygenates. Comparative microkinetic [25], and DFT calculations [26–29], indicate that the energy barrier for activation is significantly higher for the carbide route than for hydrogenation of the carbon atom in adsorbed CO. Therefore, hydrogen assisted CO dissociation has gained widespread attention in later years [30], and is the basis for the present work. It was suggested recently that water plays a key role in activation of CO by providing hydrogen to the oxygen atom of CO [31]; thereby enhancing the surface coverage of polymerization monomers CH_x. Indeed, previous SSITKA (Steady-State Isotopic Transient Kinetic Analysis) studies showed enhanced water induced surface coverage of polymerization intermediates [32], and generation of a CH_x surface pool. However, added water to the syngas feed may increase or decrease observed catalyst activity. More inert supports and large pore sizes have positive response, while medium to narrow pore size γ-alumina and silica have negative CO conversion response to water. Furthermore, there is a limit to the positive effect of water on activity. Too high amounts result in decreased activity; most likely due to oversaturation of the cobalt surface with water molecules. In a similar approach, Iglesia and co-workers suggested that water acts as a "hydrogen shuttling mediator" that facilitates hydrogenation of CO through a $H_3O^{\delta+}$ intermediate [33,34].

There are numerous published kinetic models for cobalt FTS, and surveys have been given by van Santen et al.[35], Keyvanloo et al.[36], and Ostadi et al. [37]. Some of the micro kinetic models proposed for Fischer Tropsch synthesis are by Storsæter et al.[25], Todic et al. [38], Mosayebi and Haghtalab [39], Van Santen et al. [40], and Visconti et al. [41]. The present work is based on a microkinetic approach and the Langmuir-Hinshelwood (LH)[42] formalism. The LH kinetic constants are lumped and estimated by adjustments to experimentally observed rates. Further, simplifications are made by only considering coverage of the surface by species that are expected to be most abundant.

As described above, it appears reasonable that water is participating in the rate-limiting step of FTS, either directly as adsorbed water or after dissociation to hydroxyl. Chain growth;

$$C_nH_{2n} + CH_2 \rightarrow C_{n+1}H_{2n+2}, \quad (2)$$

here approximated by a growing chain by adding a CH_2 unit, as well as chain termination, need to be addressed on a micro-kinetic scale with due consideration of the water present. A unique feature of the developed consorted vinylene mechanism is invariance of the ASF α on the partial pressure of hydrogen [31]. Indeed, Oosterbeek and van Bavel have shown that α does not change with pressure of hydrogen; when the pressure of CO is being kept constant [43].

Only a few of previously available rate expressions contain water as part of the kinetic expression; see Table 1. Each published rate expression has only been fitted to a single catalyst composition, meaning that the general applicability is questionable Two of the investigations comprise testing of added water. Only one formulation include water in the principal nominator, and then as a negative response (van Steen and Schulz [45]). Bukur, Davis, Jacobs and co-workers published three expressions for standard catalysts, but behaving opposite as to the effect of water [46,47,49]. The two additional investigations comprise water as a term in the denominator giving a negative effect on rate [44,48]. All in all, it means that only the two expressions with $-bP_{H2O}$ term in the denominator respond positively to the partial pressure of water. Addition of this term was done to fit the data and was not mechanistically based. A negative term in the denominator has no rationale in the LH formulation, as all terms define surface coverage of a given specie.

Reviews on deactivation of FT catalysts appeared a few years ago [50,51]. The papers discuss a wide variety of deactivation mechanisms comprising sintering; re-oxidation of cobalt, including surface oxidation; formation of stable compounds between cobalt and the support, e.g., cobalt aluminate; surface reconstruction; formation of carbon species on the cobalt surface; carburization; and poisoning. Only two reports on deactivation during extended testing have been found. Sasol with partners have published extensively on deactivation at industrial conditions focusing on a polycarbon deposition mechanism [52]. In contrast, Exxon scientists claim oxidation to be the most pronounced mechanism. Kliewer *et al.* studied redox transformations of cobalt catalysts by TEM in terms of agglomeration of the metal, mixed-oxide formation with the support and reversible oxidation [53]. Reactor studies supported by TEM showed that nanoscale Co particles can oxidize to CoO during FT synthesis conditions in spite of bulk thermodynamic data suggesting otherwise [54]. The propensity for oxidation is enhanced by small Co particles and high degree of CO conversion; promoting oxidative conditions due to high concentration of water vapor [6]. Thresholds for re-oxidation were studied by Tsakoumis et al. by *in situ* XANES [55]; concluding that cobalt nanoparticles in the outset should be larger than 5 nm to avoid oxidation. Sintering of cobalt sites are shown to be particularly important in the first days or weeks of an FT run [56,57,58]. Characterization of a commercial catalyst after ca. one

Table 1
Published rate equations containing water for CO consumption in Fischer-Tropsch synthesis on cobalt; excluding water assisted CO-activation [ref. 31].

Rate expression [a] $-r_{CO}$	Catalyst	Mechanism Kinetics	Conditions					Ref.
			Reactor type	**Tempera-ture (°C)**	**Pressure (bar)**	**% COconv.**	**H_2/CO feed**	
aP_{H2} / $\{1+bP_{H2O}/P_{CO}P_{H2}\}$	Co/Zr/ SiO_2	Carbide	CSTR[b]	240-280	30	n.a.	1.0-2.0	Withers et al. [44]
$a\{P_{H2}^{1.5}P_{CO}/P_{H2O}\}$ / $\{1+bP_{H2}P_{CO}/P_{H2O}\}$[2]	Co/MgO/ ThO_2/SiO_2	Carbide Micro	CSTR	190-210	2.7-6.2	n.a.	Wide + H_2O	van Steen and Schulz [45]
$a\{P_{H2}^{0.5}/P_{CO}^{0.25}\}$ / $\{1-bP_{H2O}/P_{H2}\}$	Co/ SiO_2	Empirical Macro	CSTR	210	21.6	12.2-37.7	1.0-2.4 + H_2O	Das et al. [46]
$aP_{H2}^{0.5}P_{CO}$ / $\{1-bP_{H2}^{0.5}+cP_{CO}-dP_{H2O}\}$ [2]	Co/Ru/ Al_2O_3	Carbide LH	CSTR	205-220	14-24	n.a.	1.4-2.1	Bhatelia et al. [47]
$aP_{H2}/\{1+bP_{H2}^{0.5}+cP_{CO}+dP_{H2O}/P_{H2}^{0.5}+eP_{H2O}/P_{H2}^{1.5}\}$ [2]	Co/activ. carbon	CO insertion LH	Fixed-bed	220-250	20-40	10-53	1.0-2.5	Qian et al. [48] [c]
$a\{P_{H2}^{0.88}/P_{CO}^{0.31}\}$ / $\{1-bP_{H2O}/P_{H2}\}$	Co/ Al_2O_3	Empirical Macro	CSTR	205-230	14-25	3-59	1.0-2.5	Ma et al. [49]

[a] Coefficients are positive. [b] Continuously stirred tank reactor. [c] Simplified expression for paraffins. n.a.: not available.

month operation in a 600 bpd slurry-bubble column showed initial increase in the degree of reduction of cobalt, followed by sintering attributed to crystallite migration [59]. Another sintering mechanism that has been considered is Ostwald ripening, where cobalt atoms are transported from smaller to larger crystallites [60]. It is beyond the scope of the present work to study deactivation and deactivation mechanisms *per se*, but modelling decline in observed rate is a necessity to be able to fit kinetic parameters. Handling of deactivation in the studies shown in Table 1 are summarized in Table 2. To our knowledge, no explicit expression for deactivation of a cobalt Fischer-Tropsch catalyst has been published previously; neither mechanistically based nor purely empirical.

The present work encompasses kinetic modelling of a series of rhenium promoted cobalt Fischer-Tropsch catalysts supported on γ-alumina with a large variety in pore sizes, to the inert α-alumina. Rhenium was first reported added to a Co/titania catalyst [61], and shortly after to Co/γ-alumina [62]. Mauldin and Varnado concluded that for the former system rhenium increases cobalt oxide dispersion and promote reduction of cobalt oxide [63]. The same conclusion was reached for alumina supported catalysts by Hilmen et al. [64]. Diehl and Khodakov have reviewed promotion of cobalt FT-catalysts with noble metals [65]. All in all, the present work focuses on a novel mechanism that is able to describe a multitude of cobalt Fischer-Tropsch catalysts with varying responses to water, and with a concurrent model for deactivation.

2. Experimental

2.1. Catalyst preparation

Laboratory catalysts were prepared as described previously [66,67], including one-step incipient wetness co-impregnation with an aqueous solution of cobalt nitrate hexahydrate and perrhenic acid. One α-Al_2O_3 support was prepared by calcination of γ- Al_2O_3 (Puralox SCCa). After impregnation the catalyst was dried in a stationary oven at 110-120°C for 3 h; followed by calcination at 300°C for 16 h. 6 catalysts were prepared and numbered as shown in Table 3 and in accordance with a previous study [66,68]. The C_{14} α-alumina sample corresponds to $C_{\alpha 1}$ [3]. The catalyst supports span a variety of kinetic properties where the response of water on activity is very negative (C_{11}), slightly negative (C_3), neutral (C_{10}) or positive (C_{14}). The latter catalyst has also significantly improved selectivity to C_{5+}.

2.2. Catalyst characterization

Key characterization data are found in Table 3. Powder X-ray diffraction patterns and temperature-programmed reduction (TPR) can be found in previous reports[66,67].

As shown in Table 3, the investigated catalysts span wide ranges of pore diameters, pore size distributions, and cobalt particle size; giving very different Fischer-Tropsch performances in terms of activities, selectivities and water responses.

Table 2
Implementation of deactivation in kinetic studies considering water.

Catalyst	Time on stream (h)	Deactivation type	Deactivation correction	Reference
Co/Zr/SiO_2	2188-4417	Variable	Linear interpolation	Withers et al. [44]
Co/MgO/ThO_2/SiO_2	n.a.	n.a.	n.a.	van Steen and Schulz, [45]
Co/SiO_2	350-2450	Exponential decay	Linear interpolation	Das et al., [46]
Co/Ru/Al_2O_3	n.a.	n.a.	n.a.	Bhatelia et al. [47]
Co/activ. carbon	230-1350	Considered stable	No implementation	Qian et al. [48]
Co/Al_2O_3	365-918	Linear	1.4% in 553 h	Ma et al., [49]

2.3. Fixed-bed catalyst testing

FT reactions were conducted in fixed-bed reactors of stainless steel with 10 mm inner diameter. Further details are given in previous reports [67,68]. Sieved samples (53-90 μm) were diluted with silicon carbide and reduced in situ in hydrogen at ambient pressure and 350°C. Gas flow was adjusted to give CO conversion level between 45 and 50 percent after 26 h time on stream (TOS). All experiments where run at 20 bar total pressure and 210°C. Water was vaporized and added at 4.25 bar and 7.06 bar; simulating 46 and 64% conversion at the inlet, respectively.

Liquid products were collected in a heated trap followed by a cold trap, and the gaseous product was analyzed for hydrogen, nitrogen, carbon monoxide, carbon dioxide, water, and C_1 to C_9 hydrocarbons by a gas chromatograph. Activity is reported as hydrocarbon formation rate ($g_{hydrocarbon}/(g_{catalyst}h)$) with precision ($2\sigma$) of 3%

3. Mechanistic framework

3.1. The water assisted vinylene mechanism

Present kinetic modelling is based on the consorted vinylene mechanism for cobalt Fischer-Tropsch synthesis. Key element of the mechanism is water assisted CO-activation. Description of the mechanism and derived kinetics have been reported previously [31]. There are, however, several variations to the mechanism, including activation by adsorbed water or hydroxyl, and certain variations in necessary assumptions of intermediates; notably whether formyl (CHO) is in a steady state condition or in equilibrium, and if hydroxycarbene (HCOH) is included as an intermediate. Summary of the adopted mechanism is shown in Fig. 1. Principles of the mechanism comprise the following features: the carbon atom of CO is activated by hydrogen; the oxygen atom of CO is activated by H_2O (alternatively: by OH*); formyl may dissociate spontaneously upon hydrogenation, methylidyne (CH*) is the main monomer building the chain; hydrogenation of the β-carbon of the chain completes the propagation step, whereas hydrogenation of the α-carbon atom terminates chain growth; the primary product is an α-olefin.

This formalism complies with key observations in FTS synthesis, summarized to be: the existence of a CH_x pool; water enhancing CO activation and long-chain selectivity; α-olefins as primary product; chain growth probability independent of hydrogen partial pressure. The mechanism, in its basic form, does not encompass formation of oxygenates. It can, however, easily be extended to include short chain branching and higher order alcohols by addition of methyl or hydroxyl, respectively, in the beta-position instead of hydrogen.

It is necessary to develop a kinetic expression that can model both negative and positive activity responses to added water, and also give rise to chain growth probability α that increases with partial pressure of water. In addition, α should not depend on the partial pressure of hydrogen; all other partial pressures being constant. This leaves two expressions of the six reported previously [31]; both requiring that formyl is in equilibrium with adsorbed CO. We have selected the one that does not contain hydroxycarbene as an intermediate as outlined on Fig. 1. Note that simplifications of the rate equation used should be made anyway to reduce the number of variables.

Derivation of the applied FT rate equation is given below. Water, hydrogen and carbon monoxide adsorption follow [68]

$$H_2O(g) + * \leftrightarrow H_2O* \quad K_{H2O} = \theta_{H2O}/(P_{H2O}\,\theta_v) \quad \theta_{H2O} = K_{H2O}\,P_{H2O}\,\theta_v \quad (3)$$

$$H_2(g) + 2* \leftrightarrow 2\,H* \quad K_{H2} = \theta_H^2/(P_{H2}\,\theta_v^2) \quad \theta_H = K_{H2}^{½}\,P_{H2}^{½}\,\theta_v \quad (4)$$

Table 3
Properties of investigated catalysts.

Catalyst sample	Type of support	Surface area (m^2/g)	Pore diameter (nm)	Pore volume (cm^3/g)	Pore size distribution	Co particle size (nm) [a]	Degree of reduction (%) [b]
C_3	γ-Puralox SCCa 40/195	143	7.1	0.30	Sharp	8.3	56
C_7	γ-Pural NG	136	8.2	0.30	Broad	12.4	59
C_{10}	γ-Puralox SCCa 20/190	149	11.6	0.51	Broad (Low pore size shoulder)	10.2	60
C_{11}	γ-Puralox SCCa 45/190	148	11.6	0.50	Medium broad (Slightly bimodal)	9.5	61
C_{12}	γ-Puralox TH 100-150	123	18.3	0.62	Medium broad	11.3	70
C_{14}	α-alumina (84%)	23.5	~150	~0.8	-	19.0	> 90

γ: γ-alumina.
[a] By hydrogen chemisorption. [b] By oxygen titration.

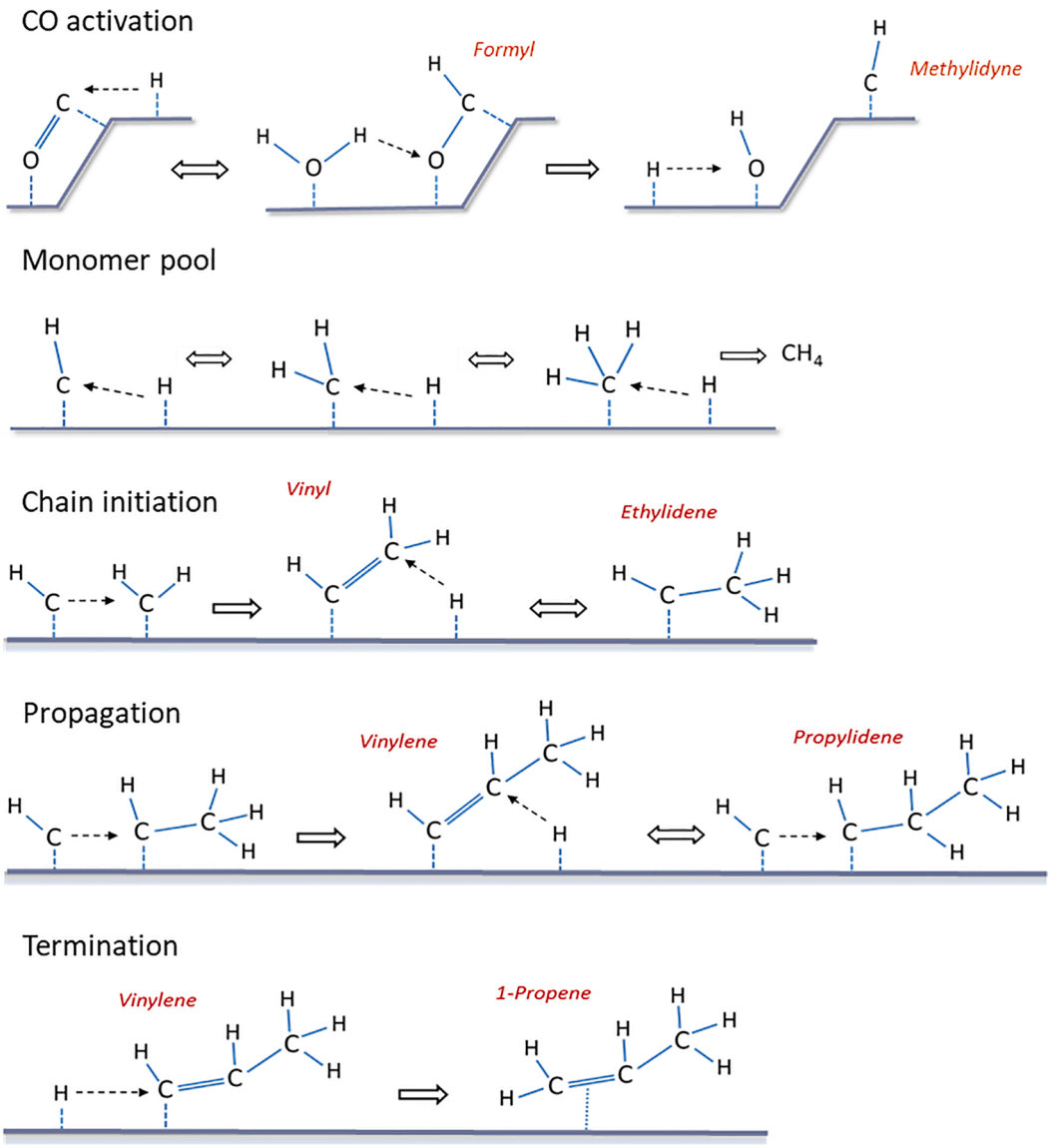

Fig. 1. CO activation, CH_x monomer pool, chain growth and termination framework on the cobalt surface.

$$CO(g) + * \leftrightarrow CO* \quad K_{CO} = \theta_{CO}/(P_{CO}\,\theta_v) \quad \theta_{CO} = K_{CO}\,P_{CO}\,\theta_v \qquad (5)$$

Adsorbed CO is assumed to be hydrogenated directly in an equilibrium reaction;

$$CO* + H* \leftrightarrow CHO* + * \quad K_{CHO} = \theta_{CHO}\,\theta_v/(\theta_{CO}\,\theta_H)$$

$$\theta_{CHO} = K_{CHO}\, K_{CO}\, K_{H2}^{½}\, P_{CO}\, P_{H2}^{½}\, \theta_v \quad (6)$$

with formation of a formyl specie. We presume that hydrogenation by H* is to a carbon atom whereas hydrogenation from H_2O* is to an oxygen atom, in accordance with the higher electronegativity of oxygen and general hydrogen bonding experience. The present mechanism calls for water activation of formyl yielding the CH* monomer as rate limiting step:

$$CHO^* + H_2O^* \rightarrow 2\ OH^* + CH^* \quad (7)$$

$$\left.\begin{aligned} r_{FT} &= -r_{CO} = r_{CH} = k_{CH}\theta_{CHO}\theta_{H_2O} \\ &= k_{CH}K_{CHO}K_{CO}K_{H_2}^{1/2}K_{H_2O}P_{CO}P_{H_2}^{1/2}P_{H_2O}\theta_v^2 \end{aligned}\right| \quad (8)$$

An estimate for the monomer CH* in the overall LH site conservation equation is included by deduction from the stoichiometry of the FT reaction; see Eqs. (1) and (2). Further CH_x, x>1, species are neglected in this context, but can easily be derived from a CH_x surface pool in equilibrium if desired. Approximately, equal amounts of water and -CH_2- chain building blocks are produced from CO. The latter can be formulated as

$$CH^* + H^* \rightarrow -CH_2-^* + * \quad (9)$$

This reaction is a confined representation of the propagation steps shown in Fig. 1. Oxygen follows the pathway CO → CHO* → OH* with depletion of CHO* as rate limiting. Therefore, by combining Eqs. (9), (8) and (4),

$$r_{\text{-}CH2\text{-}} = r_{CH}\,\theta_{CH} = (k_{CH}/k_{\text{-}CH2\text{-}})\, K_{CHO}\, K_{CO}\, K_{H2O}\, P_{CO}\, P_{H2O}\, \theta_v \quad (10)$$

and from

$$1 = \theta_{CO} + \theta_H + \theta_{CHO} + \theta_{CH} + \theta_{OH} + \theta_{H2O} + \theta_v \quad (11)$$

the water-assisted Langmuir-Hinshelwood rate equation becomes

$$r_{FT} = k\, P_{CO}\, P_{H2}^{½}\, P_{H2O}/(1 + aP_{CO} + bP_{H2}^{½} + c(P_{CO}\, P_{H2}^{½}) + d(P_{CO}\, P_{H2O}) + e(P_{H2O}/P_{H2}^{½}) + fP_{H2O})^2 \quad (12)$$

where $k = k_{CH}\, K_{CHO}\, K_{CO}\, K_{H2}^{½}\, K_{H2O}$ and the coefficients in the denominator represent coverage of the individual surface species: $a = K_{CO}\,[\theta_{CO}]$; $b = K_{H2}^{½}\,[\theta_H]$; $c = K_{CHO}\, K_{CO}\, K_{H2}^{½}\,[\theta_{CHO}]$; $d = (k_{CH}/k_{\text{-}CH2\text{-}})\, K_{CHO}\, K_{CO}\, K_{H2O}\,[\theta_{CH}]$; $e = (K_{OH}\, K_{H2O}/\, K_{H2}^{½})\,[\theta_{OH}]$; $f = K_{H2O}\,[\theta_{H2O}]$.

Eq. 12 is impractical for fitting to observed rates or conversions, and two types of modifications are made. First, the denominator is simplified to only account for surface species that are assumed to be major occupants of surface sites. The only carbon entity left is CO, and hydroxyl is deemed less important than water; meaning that terms c, d and e are removed. Second, there is a fundamental issue related to modelling of fixed-bed reactors as feeding dry syngas might mean that the reaction will not start due to the proportionality of rate with partial pressure of water. However, it is argued that there anyway is some water on the cobalt surface after reduction of cobalt oxide with hydrogen. Besides, we do not claim that the present route for activation of CO is exclusive; some initial activation can stem from other mechanisms and sites. The practical equation for modelling therefore is

$$r_{FT} = k_{FT}\, P_{CO}\, P_{H2}^{½}\, (P^{\circ} + P_{H2O})/(1 + aP_{CO} + bP_{H2}^{½} + f\, P_{H2O})^2 \quad (13)$$

with only five adjustable parameters reflecting, respectively; overall activity level, initial activity, and the stickiness of CO, hydrogen, and water. Note that the equation can account for both positive and negative effects of water depending on the parameter *f* and the partial pressure of water. In particular, overloading the catalyst with water suppresses coverage of other critical species with consequent reduction in Fischer-Tropsch rate. It is expected that *f* reflects properties of the support like inertness and pore size.

3.2. Chain propagation probability

Main effort has been put on modelling rates, but selectivities to C_{5+} and methane have been calculated as well; see the section on kinetic modelling. It is therefore of interest to derive an expression for chain growth probability from the water assisted vinylene mechanism. The chain growth selectivity, as described by the Anderson-Schultz-Flory (ASF) polymerization probability α, is

$$\alpha = r_p/(r_p + r_t) = 1/(1 + r_t/\, r_p) \quad (14)$$

where r_p is chain propagation rate and r_t is chain termination rate, or the sum of chain termination rates. In addition, separate models are required for methane and C_2 products that deviate severely from the ASF distribution. According to the present mechanism, propagation is composed of two consecutive reactions, insertion of methylidyne (-CH) into the RCH chain followed by vinylene hydrogenation:

$$r_{p(CH)} = k_{pCH}\, \theta_{RCH}\, \theta_{CH} \quad (15)$$

$$r_{p(H)} = k_{pH}\, \theta_{RCHCH}\, \theta_H, \quad (16)$$

whereas termination of RCHCH is described by

$$r_t = k_t\, \theta_{RCHCH}\, \theta_H \quad (17)$$

It appears reasonable that hydrogenation of vinylene to vinylidene is an equilibrium reaction:

$$K_{RCH2CH} = (\theta_{RCH2CH}\, \theta_v/(\theta_{RCHCH}\, \theta_H) \quad (18)$$

forcing enhanced chain growth when the insertion rate toward RCHCH increases. The resulting expression for α, with $r_p = r_{p(CH)}$, is

$$\alpha_n = 1/\{1 + (k_t\, \theta_{RCH2CH}\, \theta_v)/(k_{pCH}\, K_{RCH2CH}\, \theta_{RCH}\, \theta_{CH})\} \quad (19)$$

The expression for α is intuitively reasonable as it depends on the relative propensity for vinylene to be hydrogenated toward an α-olefin product or to a vinylidene ready for further chain growth. Living polymerization with $k_t = 0$ corresponds to α = 1. Introducing the surface coverage of CH* from Eq. 10 gives

$$\alpha_n = 1/\{1 + k_\alpha\, (\theta_{RCH2CH})/\theta_{RCH})/(P_{CO}\, P_{H2O})\} \quad (20)$$

with $k_\alpha = k_t\, /k_{pCH}\, K_{RCH2CH}\, (k_{CH}/k_{\text{-}CH2\text{-}})\, K_{CHO}\, K_{CO}\, K_{H2O}$. For two consecutive chain lengths, $\theta_{RCH2CH} \approx \theta_{RCH}$ and

$$\alpha_n \approx 1/\{1 + k_\alpha/(P_{CO}\, P_{H2O})\} \quad (21)$$

At first sight, it is astonishing that α_n does not depend on the partial pressure of hydrogen. This agrees with the work of Oosterbeek et al. [43]. It is well known that lower H_2/CO feed ratio lifts α. A reduced partial pressure in hydrogen is, however, reflected in enhanced pressures of CO and H_2O, giving the expected response. The mechanistic rationale is that more CO or H_2O is available for generation of CH* monomers meaning that θ_{CH} and the propagation rate increase. Alternative assumptions, like CHO* being in a steady state, give invariance to P_{H2O}. In practice, we adopt the following modified dependency of water, where y is a variable that accounts for the mentioned variations of the reaction mechanism:

$$\alpha_n \approx 1/\{1 + k_\alpha/(P_{CO}\, P_{H2O}^{y})\} \quad n > 1;\ 0 < y \leq 1 \quad (22)$$

3.3. Formation of methane

Formation of methane is derived similarly from surface coverages of the CH_x surface pool.

$$CH^* + H^* \leftrightarrow CH_2^* + * \quad K_{CH2} = \theta_{CH2}\, \theta_v/(\theta_{CH}\, \theta_H) \quad (23)$$

$$CH_2^* + H^* \leftrightarrow CH_3^* + * \quad K_{CH3} = \theta_{CH3}\, \theta_v/(\theta_{CH2}\, \theta_H) \quad (24)$$

$$CH_3^* + H^* \rightarrow CH_4\,(g) + 2^* \quad r_{CH4} = k_{CH4}^{'}\, \theta_{CH3}\, \theta_H \quad (25)$$

Eliminating the surface concentrations of CH_2* and CH_3* yields

$$r_{CH4} = k'_{CH4}\, K_{CH2}\, K_{CH3}\, \theta_{CH}\, \theta_H^3/\theta_v^2 \quad (26)$$

with substitutions from Eqs. (4), (10), (11) and (12);

$$r_{CH4} = r_{FT}\,(k'_{CH4}/k_{-CH2-})\, K_{CH2}\, K_{CH3}\, P_{H2} = r_{FT}\, k_{CH4}\, P_{H2} \quad (27)$$

where the explicit expression is obtained by using r_{FT} from Eq. (12) or (13).

The first propagation probability, α_1, is defined by; r_{CH4} as termination reaction, and the chain initiation reaction; see Fig. 1:

$$r_{1p} = k_{1p}\, \theta_{CH}\, \theta_{CH2}; \quad \alpha_1 = 1/\{1 + (k'_{CH4}\, K_{CH3}/k_{1p})\, (\theta_H^2/(\theta_{CH}\, \theta_v))\} \quad (28)$$

giving

$$\alpha_1 = 1/\{1 + k_{\alpha 1}\, P_{H2}/(P_{CO}\, P_{H2O})\} \quad (29)$$

where $k_{\alpha 1}$ is a function of four rate constants and five equilibrium constants. Interestingly, Eq. 29 is equivalent to the general α_n expression in Eq. 21 with the added P_{H2} dependency. This complies with the extra P_{H2} term for r_{CH4} compared to r_{FT} and complies with methane selectivity depending on the hydrogen partial pressure.

4. Kinetic modelling

4.1. Fischer-Tropsch reactions

The kinetic modelling is based on derivations described previously where components of five carbon atoms and more are lumped into two lumps, one for the paraffins and one for the olefins, while the rest are individual components:

$$r_1\text{: } CO + U_1\, H_2 \rightarrow \nu_{1,1}CH_4 + \nu_{2,1}C_2H_6 + \nu_{3,1}C_3H_8 + \nu_{4,1}C_4H_{10} + \nu_{[5,\infty],1}C_5^p + H_2O \quad (30)$$

$$r_2\text{: } CO + U_2\, H_2 \rightarrow \nu_{1,2}CH_4 + \nu_{2,2}C_2H_6 + \nu_{3,2}C_3H_8 + \nu_{4,2}C_4H_{10} + \nu_{[5,\infty],2}C_5^o + H_2O \quad (31)$$

$$r_3\text{: } CO + 3\, H_2 \rightarrow CH_4 + H_2O \quad (32)$$

$$r_4\text{: } C_2H_4 + 2\, H_2 + CO \rightarrow \Sigma\nu_{i,4}C_{2i+1}H_{2i+4} + H_2O \quad (33)$$

Here, U_1 and U_2 are consumption ratios of hydrogen uniquely defined by the stoichiometric coefficients ν and the chain propagation probabilities α_p and α_o for paraffins and olefins, respectively [69]. The relationship between these stoichiometric equations and the mechanistic framework developed above is the following:

r_1: The rate for reaction r_1 making paraffins is approximated by r_{FT} of Eq. 13 with the chain propagation probability given by α_n of Eq. 22 using the notations r_{FT}^p and α_n^p.
r_2: Similarly, the olefin rate for reaction r_2 also is approximated by r_{FT} of Eq. 13 with the chain propagation probability given by α_n of Eq. 22, but now using the notations r_{FT}^o and α_n^o. Scaling factors are used such that

$$r_{FT}^o = 0.1\, r_{FT}^p \text{ and } \alpha_n^o = \alpha_n^p\, e^{-0.27}. \quad (34)$$

r_3: Methane rate is modelled by Eq. 27, but with subtraction of the methane already accounted for by the reactions of Eqs. 30 and 31.
r_4: Reaction for further insertion and polymerization of ethene is applied to account for the abnormally very low concentration of C_2 components; but do not rely on a specific mechanism. In fact, an alternative possibility is that the C_2 intermediate is less prone to termination for energetic reasons and preferably proceed to chain initiation; see Fig. 1.

$$r_{C2} = 0.5\, P_{CO}{}^*P_{C2H4}{}^*P_{H2}^2 \text{ (rate constant} = 0.25 \text{ for } C_{14}); \alpha_{C2} = 0.7\, \alpha_n^p. \quad (35)$$

Note that in the present simulations, formation of olefins and paraffins are modelled as the individual reactions r_1 and r_2 and are not linked to any detailed mechanism like paraffins being a secondary product of hydrogenation. This is of no consequence for the focus of the present work; fitting CO conversion, and C_{5+} and CH_4 selectivities, to observed data and testing key elements of the mechanism.

4.2. Deactivation

To model real data, deactivation has to be taken into account. We have implemented a conceivably simple deactivation function

$$da/dt = -k_d\, a^n\, P_{H2O}^\gamma \text{ with } n = 2;\ \gamma \approx 1 \quad (36)$$

with only one variable parameter, k_d, that changes from catalyst to catalyst. As shown below, this parameter describes the data well. Although a detailed mechanistic interpretation of deactivation is not under scrutiny, the a^2 term can be visualized as sintering where two cobalt sites collapse into one, while P_{H2O} takes care of cobalt oxidation under enhanced water vapor pressures:

$$Co^* + Co^* \rightarrow 2Co^* \text{ and } Co^* + H_2O \rightarrow CoO + H_2 \quad (37)$$

5. Results and discussion

5.1. Activity response

The investigated γ-alumina supports span a variety in pore sizes and pore size distributions as these characteristics severely influence both selectivity and water responses; see the Introduction and references [3, 66]. Experimental and modelled activity responses for the narrow pore catalyst C_3 are compared in Fig. 2. Conversion is lifted to 50% from period A to B by adjusting Gas-Hourly-Space-Velocity (GHSV). The observed deactivation in period B is accelerated by adding water in period C and even more by adding a significant amount of water in period D. Note the abrupt negative response to water in the start of these periods, showing that the coefficient *f* of Eq. 13 outweighs the positive water response in the nominator of the equation. Returning to the initial conditions of period B in period E quantifies the deactivation of the interjacent periods, and shows that deactivation is reduced as the reaction proceeds. According to the model, the main cause of deactivation is oxidation in the periods where water is added, and sintering in the dry syngas periods. It is gratifying that the observed conversion is captured

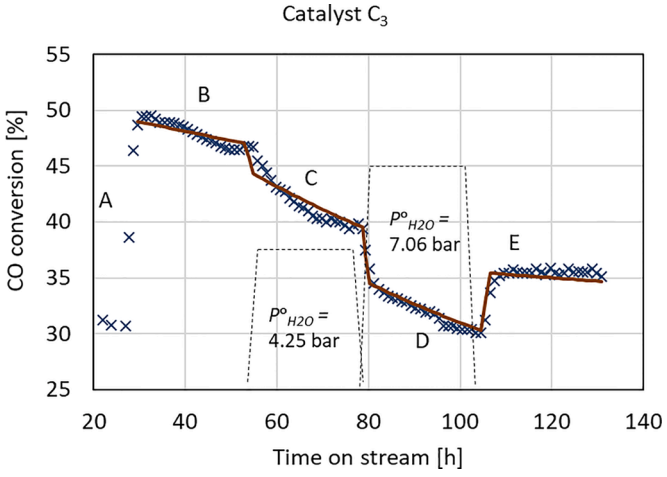

Fig. 2. CO conversion for catalyst C_3. Crosses: experimental data. Line: model.

well by using the water assisted vinylene mechanism and a simplified deactivation model. Some deviations are seen in the beginning of each period, most noticeable for period C, that are ascribed to slow diffusion of water into the pores of the catalyst until a steady gas composition is attained. Added water feed is stopped at the start of period E.

That the present mechanistic framework is capable of modelling activity responses for catalysts with different pore structures and on different substrate materials is illustrated in Fig. 3. For all the catalysts a reasonable fit is achieved. Catalyst C_{14} on α-alumina, and to a minor extent catalyst C_{10}, show positive responses to added water in period C, while excess water in period D evidently overloads the cobalt surface with water; leaving too little space for hydrogen and CO. The water assisted CO dissociation model supports previously reported trends in water response [2]. Period C indicates that FT-activity improves with water concentration,

- as pores becomes larger,
- as the pore size distribution becomes narrower, and
- as the support becomes more inert, e.g., γ-alumina → α-alumina.

Therefore, we infer that activity responds positively to water for more inert supports, this originating in the material composition or in the crystallite size. Note that narrow pores are associated with smaller alumina crystallites and higher roughness of the surface. The mentioned overloading with possible condensation of water, i.e., period D and possibly period C for catalyst C_3, is expected to be more severe for narrow pores and surfaces containing high concentration of hydroxyl groups.

5.2. Deactivation

The deactivation function of Eq. 36 is analyzed further in Fig. 4. Upper curves show deactivation as modelled; supporting the previous statements of accelerated deactivation when water is added. Expected relaxed deactivation with TOS is seen by comparing period E with period B. At first sight, it is astonishing that the deactivation rate is practically unchanged when going from the first to the second water addition period, i.e., from period C to D, with larger addition of water to the syngas. One possible explanation is that water condenses giving no additional change in fugacity. After all, the water vapor pressure is 7 bar at the inlet to the reactor, increasing typically to 10.5 bar at the exit in period D; meaning more than half the total pressure. An additional factor is self-compensation as the deactivation rate is reduced when the catalyst already is deactivated; both due to lower water vapor pressure at lower conversion levels, and that the catalyst becomes less prone to sintering and oxidation with time. Deactivation evidently also depends on the catalyst formulation. As might be expected, the catalyst on α-alumina, C_{14}, deactivates the least. This catalyst has the largest and most regular crystallites suppressing both oxidation and sintering, in contrast to catalysts C_{10} and C_{11} (yellow and blue lines). It is highly surprising that the catalyst on narrow pore γ-alumina, with the smallest and presumably most distorted cobalt crystallites, C_3, has deactivation comparable to C_{14}. Previously we attributed abnormal behavior of the C_3 catalyst to condensation of water in narrow pores [2]. Indeed, this interpretation falls in line with the statement above that condensation of water can suppress deactivation.

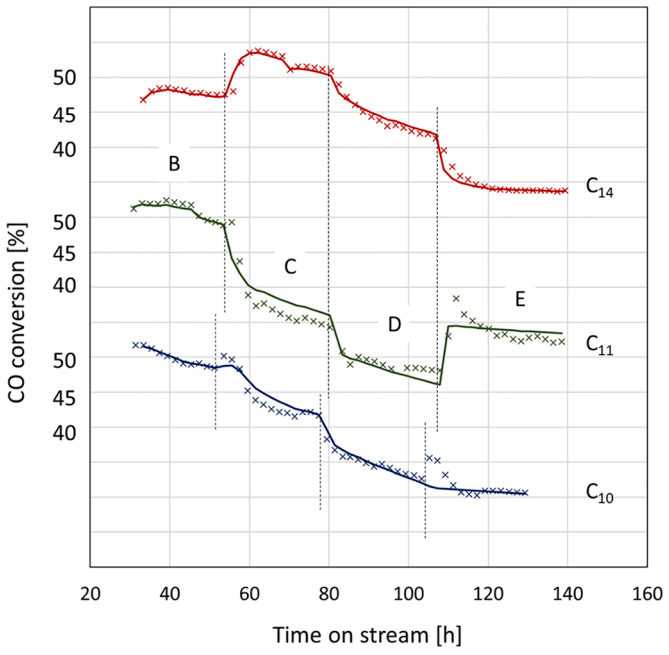

Fig. 3. CO conversion for catalysts C_{10}, C_{11} and C_{14}. Crosses: experimental data. Line: model.

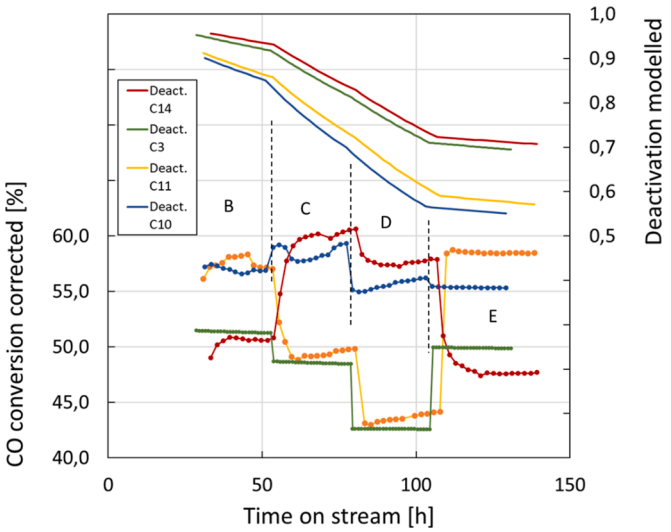

Fig. 4. Modelled deactivation of investigated catalysts (upper half) and resulting conversion corrected for deactivation.

Observed conversion corrected for deactivation is shown in the bottom half of Fig. 4. Now, the qualitative statements on how the different catalysts respond to water addition becomes self-evident. First, let us re-establish that crowding the surface with water in period D suppresses syngas conversion. Still, the effect is moderate for catalysts C_{14} and to some extent for C_{10}. Significant differences with catalyst support are exhibited in period C with more moderate water addition to syngas. The most significant conclusion is that the α-alumina supported catalyst C_{14} responds very favorably to water; on par with titania as support [70]. Further, it is evident that γ-alumina can give rise to very different behavior of the catalyst with respect to water. In other words, there is no universal γ-alumina supported catalyst or properties that can be ascribed to γ-alumina. These variations for γ-alumina based catalysts are highlighted when comparing catalysts C_{10} and C_{11}; two catalysts with similarities in overall average characteristics, see Table 3, but with very different performances.

Additional insight into deactivation is attempted in Fig. 5 where the derived deactivation rate constant, k_d, is plotted as a function of cobalt dispersion. Note that it has been possible to assign a single value for k_d through the entire experimental sequence for a given catalyst. This constant is compared with the space velocity needed to achieve 50% CO conversion. There is approximate linear correlation between GHSV and cobalt dispersion, indicating that the turn-over-frequency (TOF) per exposed cobalt atom is constant. The lower-than-expected GHSV needed for C_3 complies with detected structure sensitivity for Co FT-catalysts observed for crystallite sizes below 8 nm [71]. As foreseen,

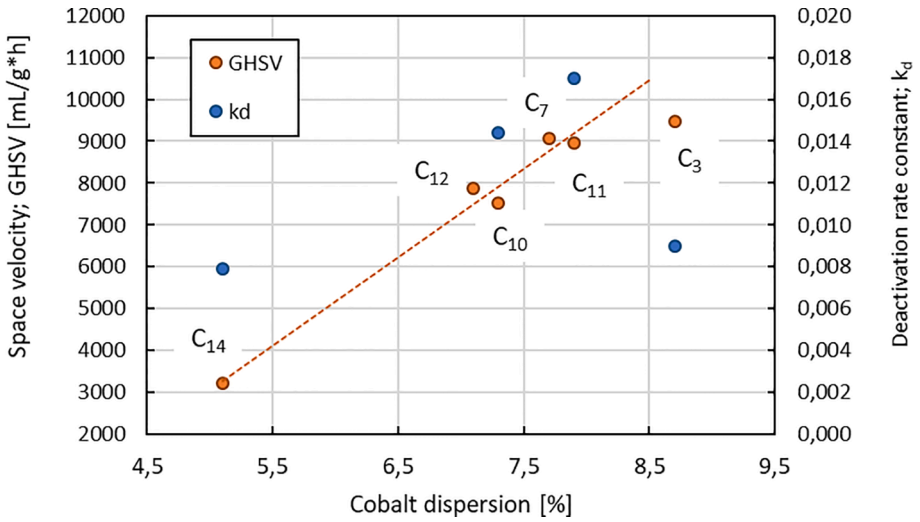

Fig. 5. Deactivation rate constant k_d and gas-hourly-space-velocity as a function of cobalt dispersion measured by hydrogen chemisorption.

deactivation increases with dispersion, i.e., when cobalt is well dispersed on the surface of the support and more exposed to sintering and oxidation. Again, the disruption for C_3 is evident.

5.3. Selectivity

Selectivities to methane an C_{5+} are compared in Figs. 6–9 for the four catalysts. The model fit represents the experimental values rather well in light of the large variation in catalyst properties, experimental conditions during a run and the deactivation that takes place. For all changes in experimental conditions, i.e., going from one of the periods A-D to the next period, the responses on methane and C_{5+} are reciprocal. This is partly a consequence of the carbon balance, but not entirely. Most remarkable is the ability of the mechanism to represent these variations with an expression for the chain propagation probability α that does not contain the partial pressure of hydrogen. Another feature of both the experimental data and the model prediction is that addition of water to the reactor in period C improves the selectivity to C_{5+}, and reduces the selectivity to methane; even more so in period D with higher water level.

Deactivation was analyzed in some detail above, and we now also experience a significant impact of deactivation on selectivities. Most distinct is the effects in periods B and C. In period B it is expected that

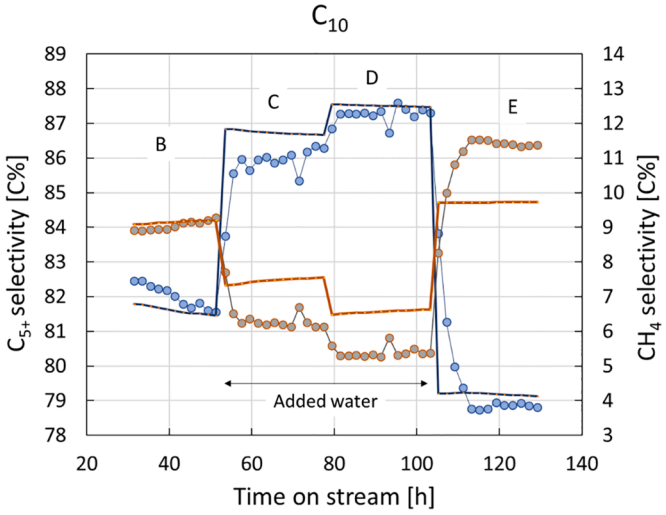

Fig. 7. Comparison of experimental (circles) and modelled (solid line) selectivities to C_{5+} (blue) and CH_4 (brown) for catalyst C_{10}.

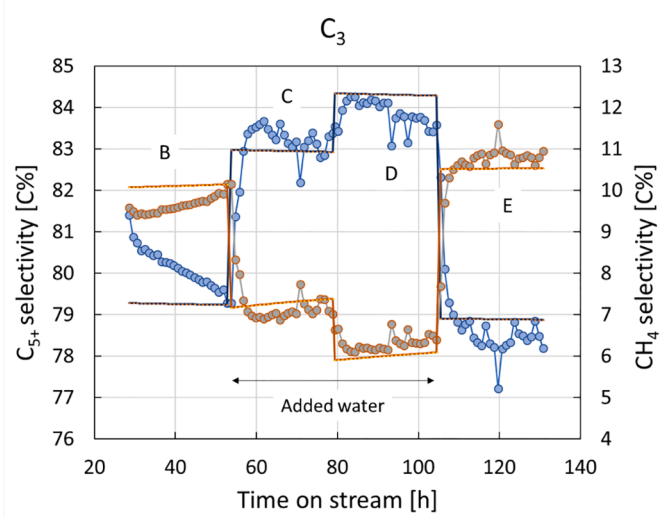

Fig. 6. Comparison of experimental (circles) and modelled (solid line) selectivities to C_{5+} (blue) and CH_4 (brown) for catalyst C_3.

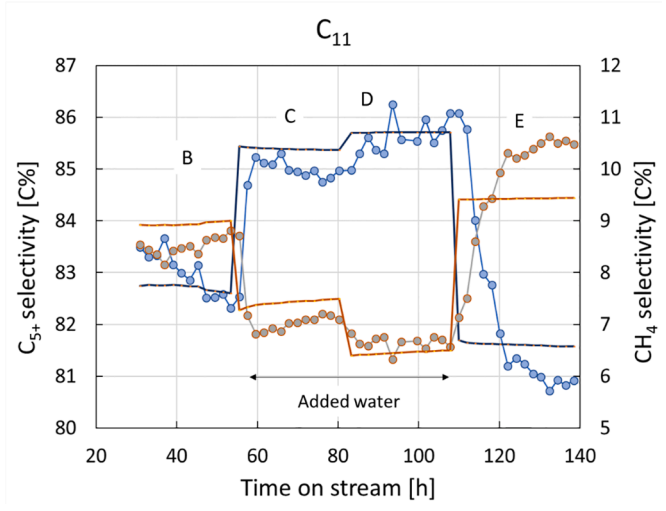

Fig. 8. Comparison of experimental (circles) and modelled (solid line) selectivities to C_{5+} (blue) and CH_4 (brown) for catalyst C_{11}.

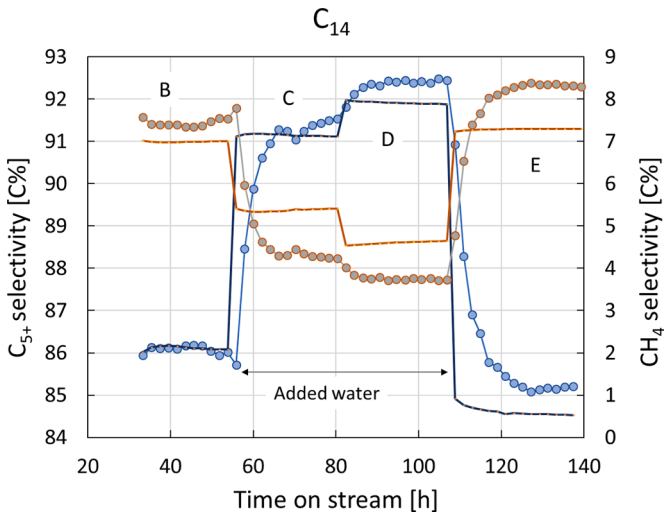

Fig. 9. Comparison of experimental (circles) and modelled (solid line) selectivities to C_{5+} (blue) and CH_4 (brown) for catalyst C_{14}.

sintering is the main mechanism, while oxidation plays a significant role in period C. Sintering reduces the C_{5+} selectivity for catalysts C_3, C_{10} and C_{11}, see Figs. 6–8. The effect is very significant for catalyst C_3 as is expected from the small average Co crystallite size of this catalyst; *cf.* Table 3. In contrast, no sintering is observed for catalyst C_{14} on α-alumina support; Fig. 9. This apparent lack of sintering is expected from the large Co crystallite size of 19 nm, but alternatively follows from the structure insensitivity to cobalt crystallite size in the region from 15 nm and above. In fact, the effect of Co crystallite size on selectivities was studied previously is some detail. It was found, for γ-alumina as catalyst support, that the C_{5+} selectivity increases from 3 nm to 8 nm, followed by decrease to ca. 12 nm, followed by leveling out for larger crystallites [72]. Thus, the present observations are in good compliance with literature data. Structure sensitivity from sintering is also apparent in the CO-conversion plots on Figs. 2 and 3 where catalyst C_3 shows largest effect and C_{14} the least. All data are on the right-hand side of the volcano plot for TOF as a function of Co size [72]. There is also a minor synergistic effect in that lower conversion produces less water that again has a negative effect on production of higher hydrocarbons.

The present selectivity model does not include any correction for deactivation and, therefore, some deviations from experimental data are expected. The model catches variations in CO-conversion; see the downward trend of the C_{5+} line in period B (Fig. 7), and the difference in selectivity between periods B and E. On the other hand, it has presently not been possible to include sintering or oxidation as part of the selectivity simulations. It follows that largest deviations between experiments and model predictions in period E are found for the most deactivated catalysts C_{10} and C_{11}. The effect on selectivity by the strong deactivation in period C is less evident, partly due to overlapping with a transient period where water diffuses into the pores of the catalyst.

5.4. Parameter estimation

The estimated parameters are summarized in Table 4. These encompasses the overall rate constant $\mathbf{k_{FT}}$; CO and hydrogen coverage parameters **a** and **b**, respectively, with **a** kept constant; direct water parameter **f** for water coverage; $\mathbf{P_{H2O}°}$ for initial water concentration; **y** for water sensitivity of α; rate constant $\mathbf{k_{CH4}}$ for methane formation; deactivation constant $\mathbf{k_d}$; and chain termination to propagation constant $\mathbf{k_\alpha}$. The initial observation is that all constants have reasonable values. In contrast to other reports on kinetics, there is no need for extreme values to fit the data. No negative parameters are inferred from the fitting algorithm. However, due to the complex relationships to individual rate constants for specific reactions, adsorption coefficients and equilibrium constants, no attempt has been made to deduce such fundamental data.

Table 4
Estimated kinetic model parameters for Fischer-Tropsch synthesis based on the vinylene mechanism. Parameters directly coupled to the partial pressure of water are f, P and y [a].

Parameter	Catalyst			
	C3	**C10**	**C11**	**C14**
$\mathbf{k_{FT}}$	1.68	1.56	2.13	1.17
a	3.5	3.5	3.5	3,5
b	1.50	1.0	1.15	1.67
f	0.103	1.24	1.86	1.06
$\mathbf{P_{H2O}°}$	1	0.94	0.67	0.49
$\mathbf{k_{CH4}}$	0,107	0,096	0,094	0,071
$\mathbf{k_d}$	0.0090	0.0170	0.0144	0.0079
$\mathbf{k_\alpha}$	0.057	0.024	0.0033	0.0102
y	0.107	0.422	0.252	0.60
GHSV (mL/g*h) @ 50% conv.	9480	8947	7536	3231

[a] Units are based on reaction rates in $g_{hydrocarbon}/g_{cat}$*h and pressures in bar.

It is worthwhile to analyze some of the parameters in detail. The three parameters reflecting the effect of water are plotted in Fig. 10 for the four catalysts at hand. The linear relationships for $\mathbf{P_{H2O}°}$ and **y** with dispersion, i.e., inverse cobalt crystallite size based on hydrogen chemisorption, is remarkable. Evidently, the lowest initial water pressure $\mathbf{P_{H2O}°}$ is needed for C_{14}; large crystallites require low GHSV for 50% conversion (Table 4), and therefore might be less sensitive to start-up conditions. However, it should be realized that the model is based on steady-state conditions, and the mechanism cold be somewhat different during start-up. Simultaneously, the large well-shaped cobalt crystallites of C_{14} respond most strongly to water vapor pressure, parameter **y**, for the ASF α-value. Recall that α does not depend on the hydrogen partial pressure, but is favored by conditions that facilitate activation of CO with subsequent production of CH* monomers. It appears as if water is most effective for activation of CO when there is a well-defined lateral surface of cobalt. The variations in the water coverage parameter **f** are more erratic. Nevertheless, it is consistent with the other observations for the high dispersion catalyst C_3 that water plays a minor role when it presumably is in condensed form.

6. Conclusions

- The water assisted vinylene mechanism for cobalt Fischer-Tropsch synthesis have been detailed for CH* as monomer and expanded to include selectivity to methane.

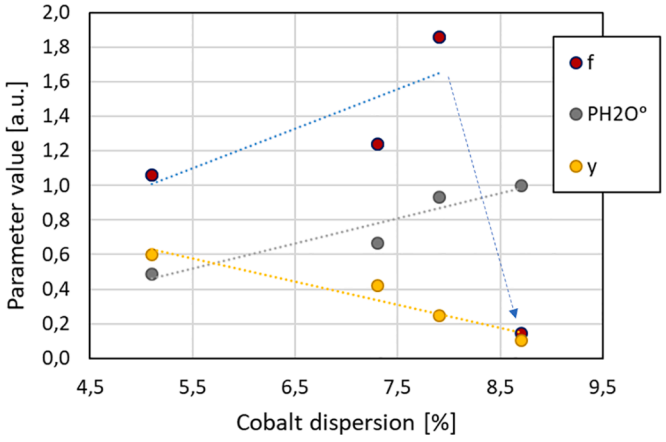

Fig. 10. Comparison of estimated kinetic parameters for cobalt FT catalysts C_3, C_{10}, C_{11} and C_{14} encompassing the direct water sensitive parameters f, $P_{H2O}°$ and y.

- Langmuir-Hinshelwood kinetic expression has been developed based on formyl in equilibrium with CO and direct dissociation of formyl with water.
- The selected mechanism follows from the associated chain propagation probability α being independent of hydrogen partial pressure, but dependent on water partial pressure.
- Activity data for 4 FT-catalyst with varying properties have been corrected for deactivation using a sintering/oxidation model.
- Derived deactivation constant for sintering correlates with cobalt dispersion; except for a narrow pore alumina where condensation of water appears to inhibit deactivation.
- Kinetic simulations for CO-conversion, C_{5+} selectivity and methane selectivity show good fit with experimental data.
- In particular, the effect of indigenous and added water is well described by the model.

The C_{5+} selectivity response to water follows inversely cobalt dispersion; large cobalt crystallites respond more positively to water. This is caught in the adjustable water parameter in the expression for α.

Justification for publication

We find this journal to be of high quality and very suitable for publishing the work as it contains both mechanistic features, kinetics, experimental work and modelling, including deactivation. It therefore is both of fundamental nature and contains useful insight and formulations for application of Fischer-Tropsch (FT) synthesis.

Novel aspects of the work comprise:

- Full mechanistic (LH) formulation of the previously proposed vinylene mechanism for cobalt FT synthesis, including reaction rate, the α-chain propagation probability, and methane selectivity.
- First expression and kinetic modelling that take into account both positive and negative effects of produced water for FT-synthesis.
- First multi catalyst FT kinetic modelling; includes a large variety of responses to process conditions.
- First kinetic FT modelling that includes mechanistic based deactivation mechanisms.

Data availability

Data will be made available on request.

CRediT authorship contribution statement

Erling Rytter: Conceptualization, Methodology, Writing – original draft, Visualization. **Anders Runningen:** Formal analysis, Investigation. **Edd Blekkan:** Validation, Supervision, Project administration, Funding acquisition. **Magne Hillestad:** Methodology, Supervision, Resources.

Declaration of Competing Interest

The authors declare that they have no known competing financial interests or personal relationships that could have appeared to influence the work reported in this paper.

Acknowledgements

Financial support from The Research Council of Norway under Contracts no. 228741 and 280846 is gratefully acknowledged. The experimental work was conducted by Øyvind Borg in connection with his Ph.D. thesis as reported previosly [3,67,68,74]. The present work relies on the actual recorded reaction profiles as TOS.

References

[1] E. Rytter, A. Holmen, Perspectives on the effect of water in cobalt Fischer-Tropsch synthesis, ACS Catal. 7 (8) (2017) 5321–5328.
[2] E. Rytter, N. Tsakoumis, A. Holmen, Water as key to activity and selectivity in Co Fischer-Tropsch synthesis: γ–alumina based structure-performance relationships, J. Catal. 365 (2018) 334–343.
[3] E. Rytter, Ø. Borg, B.C. Enger, A. Holmen, α-alumina as catalyst support in Co Fischer-Tropsch synthesis and the effect of added water; encompassing transient effects, J. Catal. 373 (2019) 13–24.
[4] S. Storsæter, Ø. Borg, E.A. Blekkan, B. Tøtdal, A. Holmen, Fischer-Tropsch synthesis over Re-promoted Co supported on Al_2O_3, SiO_2 and TiO_2: effect of water, Catal. Today 100 (2005) 343–347.
[5] G. Jacobs, T.K. Das, P.M. Patterson, J. Li, L. Sanches, B.H. Davis, Fischer-Tropsch synthesis: XAFS studies of the effect of water on a Pt-promoted Co/Al_2O_3 catalyst, Appl. Catal. A 247 (2003) 335–343.
[6] D. Schanke, A.-M. Hilmen, E. Bergene, K. Kinnari, E. Rytter, E. Ådnanes, A. Holmen, Study of the deactivation mechanism of Al_2O_3-supported cobalt Fischer-Tropsch catalyst, Catal. Lett. 34 (1995) 269–284.
[7] E.A. Blekkan, Ø. Borg, V. Frøseth, A. Holmen, A. Fischer-Tropsch, synthesis on cobalt catalysts: the effect of water. Catalysis, The Royal Society, Cambridge, UK, 2007, pp. 13–32, vol.20.
[8] N.E. Tsakoumis, E. Patanou, S. Lögdberg, R.E. Johnsen, R. Myrstad, W. van Beek, E. Rytter, E.A. Blekkan, Structure-performance relationships on Co based Fischer-Tropsch synthesis catalysts; the more defect free the better, ACS Catalysis, ACS Catal. 9 (2019) 511–520.
[9] S. Krishnamoorthy, M. Tu, M.P. Ojeda, D. Pinna, E. Iglesia, An investigation of the effects of water on rate and selectivity for the Fischer-Tropsch synthesis on cobalt-based catalysts, J. Catal. 211 (2002) 422–433.
[10] R.B. Anderson, R.A. Friedel, H.H. Storch, Fischer-Tropsch reaction mechanism involving stepwise growth of carbon chain, J. Chem. Phys. 19 (1951) 313–319.
[11] A.M. Saib, M. Claeys, E. van Steen, Silica supported cobalt Fischer-Tropsch catalysts: effect of pore diameter of support, Catal. Today 71 (2002) 395–402.
[12] L. Fratalocchi, C.G Visconti, L. Lietti, G. Groppi, E. Tronconi, E. Roccaro, R. Zennaroi, On the performance of a Co-based catalyst supported on modified γ-Al_2O_3 during Fischer-Tropsch synthesis in the presence of co-fed water, Catal. Sci. Technol. 6 (2016) 6431–6440.
[13] F. Fischer, H. Tropsch, Uber die Herstellung synthetischer olgemische durch Aufbau aus Kohlenoxyd und Wasserstoff, Brennst. Chem. 7 (1926) 97–104.
[14] A.T. Bell, Catalytic synthesis of hydrocarbons over group VIII metals. A discussion of the reaction mechanism, Catal. Rev. Sci. Eng. 23 (1981) 203–232.
[15] M.E. Dry, Practical and theoretical aspects of the catalytic Fischer-Tropsch process, Appl. Catal. A 138 (1996) 319–344.
[16] S.A. Eliason, C.H. Bartholomew, Reaction and deactivation kinetics for Fischer-Tropsch synthesis on unpromoted and potassium-promoted iron catalysts, Appl. Catal. A 186 (1999) 229–243.
[17] R. Quyoum, V. Berdini, L.M. Turner, C.H. Long, M.P. Maitlis, Mechanistic studies of methylene chain propagation in the Fischer–Tropsch synthesis, J. Catal. 173 (1998) 355–365.
[18] J. Gaube, H.F. Klein, Further support for the two-mechanisms hypothesis of Fischer–Tropsch synthesis, Appl. Catal. A 374 (2010) 120–125.
[19] G.P. van der Laan, A.A.C.M. Beenackers, Intrinsic kinetics of the gas-solid Fischer-Tropsch and water gas shift reactions over a precipitated iron catalyst, Appl. Catal. A 193 (2000) 39–53.
[20] W.K. Hall, R.J. Kokes, P.H. Emmett, Mechanism studies of the Fischer-Tropsch synthesis: the incorporation of radioactive ethylene, propionaldehyde and propanol, J. Am. Chem. Soc. 82 (1960) 1027–1037.
[21] H. Pichler, H. Schulz, Neuere Erkenntnisse auf dem Gebiet der Synthese von Kohlenwasserstoffen aus CO und H_2, Chem. Ing. Technol. 42 (1970) 1162–1174.
[22] J.P. Hindermann, G.J. Hutchings, A. Kiennemann, Mechanistic aspects of the formation of hydrocarbons and alcohols from CO hydrogenation, Catal. Rev. Sci. Eng. 35 (1993) 1–127.
[23] M. Zhuo, K.F. Tan, A. Borgna, M. Saeys, Density functional theory study of the CO insertion mechanism for Fischer-Tropsch synthesis over Co catalysts, J. Phys. Chem. C 113 (2009) 8357–8365.
[24] H.H. Storch, N. Golumbic, R.B. Anderson, The Fischer–Tropsch and related syntheses, Wiley, New York, 1951.
[25] S. Storsæter, D. Chen, A. Holmen, Microkinetic modelling of the formation of C_1 and C_2 products in the Fischer-Tropsch synthesis over cobalt catalysts, Surf. Sci. 600 (2006) 2051–2063.
[26] C.F. Huo, Y.W. Li, J. Wang, H. Jiao, Formation of CH_x species from CO dissociation on double-stepped Co(0001): exploring Fischer-Tropsch mechanism, J. Phys. Chem. C 112 (2008) 14108–14116.
[27] O.R. Inderwildi, S.J. Jenkins, D.A. King, Fischer-Tropsch mechanism revisited: alternative pathways for the production of higher hydrocarbons from synthesis gas, J. Phys. Chem. C 112 (2008) 1305–1307.
[28] M. Ojeda, R. Nabar, A.U. Nilikar, A. Ishikawa, M. Mavrikakis, E. Iglesia, CO activation pathways and the mechanism of Fischer-Tropsch synthesis, J. Catal. 272 (2010) 287–297.
[29] P. van Helden, J.A. van den Berg, Ciobica I.M, Hydrogen-assisted CO dissociation on the Co(211) stepped surface, Catal. Sci. Technol. 2 (2012) 491–494.
[30] C.G. Visconti, E. Tronconi, L. Lietti, P. Forzatti, S. Rossini, R. Zennaro, Detailed kinetics of the Fischer-Tropsch synthesis on cobalt catalysts based on H-assisted CO activation, Top. Catal. 54 (2011) 786–800.

[31] E. Rytter, A. Holmen, Consorted vinylene mechanism for cobalt Fischer-Tropsch synthesis encompassing water or hydroxyl assisted CO-activation, Topics Catal. 61 (2018) 1024–1034.

[32] C.J. Bertole, C.A. Mims, G. Kiss, Support and rhenium effects on the intrinsic site activity and methane selectivity of cobalt Fischer-Tropsch catalysts, J. Catal. 221 (2004) 191–203.

[33] S. Krishnanmoorthy, M. Tu, M.P. Ojeda, D. Pinna, E. Iglesia, An investigation on the effects of water on the rate and selectivity for the Fischer-Tropsch synthesis on cobalt-based catalysts, J. Catal. 211 (2) (2002) 422–433.

[34] D.D. Hibbits, B.T. Loveless, M. Neurock, E. Iglesia, Mechanistic impact of water during Fischer-Tropsch synthesis on Ru catalysts, Angew. Chem. Int. Ed. 20 (2013) 12273–12278.

[35] R.A. van Santen, A.J. Markvoort, M.M. Ghouri, P.A.J. Hilbers, E.J.M. Hensen, Monomer formation model versus chain growth model of the Fischer-Tropsch reaction, J. Phys. Chem. C 117 (2013) 4488–4504.

[36] K. Keyvanloo, S.J. Lanham, W.C. Hecker, Kinetics of Fischer-Tropsch synthesis on supported cobalt: effect of temperature on CO and H_2 partial pressure dependencies, Catal. Today 270 (2016) 9–18.

[37] M. Ostadi, E. Rytter, M. Hillestad, Evaluation of kinetic models for Fischer-Tropsch cobalt catalysts in a plug flow reactor, Chem. Eng. Res. Des. 114 (2016) 236–246.

[38] B. Todic, W. Ma, G. Jacobs, B.H. Davis, D.B. Bukur, CO-insertion mechanism based kinetic model of the Fischer-Tropsch synthesis reaction over Re-promoted Co catalyst, Catal. Today 228 (2014) 32–39.

[39] A. Mosayebi, A. Haghtalab, The comprehensive kinetic modeling of the Fischer-Tropsch synthesis over Co@Ru/g-Al_2O_3 core-shell structure catalyst, Chem. Eng. J. 259 (2015) 191–204.

[40] R.A. van Santen, A.J. Markvoort, I.A.W. Filot, M.M. Ghouri, E.J.M. Hensen, Mechanism and micro-kinetics of the Fischer-Tropsch reaction, Phys. Chem. Chem. Phys. 15 (2013) 17038–17063.

[41] C.G. Visconti, E. Tronconi, L. Lietti, R. Zennaro, P. Forzatti, Development of a complete kinetic model for the Fischer-Tropsch synthesis over Co/Al_2O_3 catalysts, Chem. Eng. Sci. 62 (2007) 5338–5343.

[42] M.A. Vannice, Kinetics of Catalytic Reactions, Springer, New York, 2005.

[43] H. Oosterbeek, A.P. van Bavel, Effect of CO coverage on the product slate in FTS, in: Extended abstract 992, 11th Natural Gas Conversion Symposium, 5-9 June, Tromsø, Norway, 2016.

[44] H.P. Withers Jr., K.F. Eliezer, J.W. Mitchell, Slurry-phase Fischer-Tropsch synthesis and kinetic studies over supported cobalt carbonyl derived catalysts, Ind. Eng. Chem. Res. 29 (1990) 1807–1814.

[45] E. van Steen, H. Schulz, Polymerisation kinetics of the Fischer-Tropsch CO hydrogenation using iron and cobalt-based catalysts, Appl. Catal. A 186 (1999) 309–320.

[46] T.K. Das, W.A. Conner, J. Li, G. Jacobs, M.E. Dry, B.H. Davis, Fischer-Tropsch synthesis: kinetics and effect of water for a Co/SiO_2 catalyst, Energy Fuels 10 (2005) 1430–1439.

[47] T. Bhatelia, W. Ma, G. Jacobs, B.H. Davis, D.B. Bukur, Kinetics of the Fischer-Tropsch reaction over a Ru promoted Co/Al_2O_3 catalyst, Chem. Eng. Trans. 25 (2011) 707–712.

[48] W. Qian, H. Zhang, W. Ying, D. Fang, The comprehensive kinetics of Fischer-Tropsch synthesis over a Co/AC catalyst on the basis of CO insertion mechanism, Chem. Eng. J. 228 (2013) 526–534.

[49] W. Ma, G. Jacobs, D.E. Sparks, R.L. Spicer, B.H. Davis, J.L.S. Klettlinger, C.H. Yen, Fischer-Tropsch synthesis: kinetics and water effect study over 25%Co/Al_2O_3 catalysts, Catal. Today 228 (2014) 158–166.

[50] N.E. Tsakoumis, M. Rønning, Ø. Borg, E. Rytter, Deactivation of cobalt-based Fischer-Tropsch catalysts: a review, A. Holmen, Catal. Today 154 (2010) 162–182.

[51] E. Rytter, A. Holmen, Deactivation and rejuvenation of commercial type Fischer-Tropsch Co-catalysts. A mini-review, Catalysts 5 (2015) 478–499.

[52] D.J. Moodley, J. van de Loosdrecht, A.M. Saib, M.J. Overett, A.K. Datye, J. W. Niemantsverdriet, Carbon deposition as a deactivation mechanism of cobalt-based Fischer-Tropsch synthesis catalysts under realistic conditions, Appl. Catal. A 354 (2009) 102–110.

[53] C.E. Kliever, G. Kiss, G.J. DeMartin, Ex situ transmission electron microscopy: a fixed-bed approach, Microsc. Microanal. 12 (2006) 135–144.

[54] O. Kubaschewski, C.B. Alcock, Metallurgical Thermochemistry, 5th ed., Pergamon, New York, 1979.

[55] N.E. Tsakoumis, J.C. Walmsley, M. Rønning, W. van Beek, E. Rytter, A. Holmen, Evaluation of reoxidation thresholds for γ-Al_2O_3-supported cobalt catalysts under Fischer-Tropsch synthesis conditions, J. Am. Chem. Soc. 139 (2017) 3706–3715.

[56] M. Sadeqzadeh, J. Hong, P. Fongarland, D. Curulla-Ferré, F. Luck, J. Bousquet, D. Schweich, A.Y. Khodakov, Mechanistic modeling of cobalt-based catalyst sintering in a fixed bed reactor under different conditions of Fischer-Tropsch synthesis, Ind. Eng. Chem. Res. 51 (2012) 11955–11964.

[57] M. Sadeqzadeh, S. Chambrey, S. Piché, P. Fongarland, F. Luck, D. Curulla-Ferré, D. Schweich, J. Bousquet, A. Khodakov, Deactivation of a Co/Al_2O_3 Fischer-Tropsch catalyst by water-induced sintering in slurry reactor: Modeling and experimental investigations, Catal. Today 215 (2013) 52–59.

[58] B.H. Davis, E. Iglesia, Technology development for iron and cobalt Fischer-Tropsch catalysts; Final technical report, Univ. Kentucky Research Foundation, June 30, 2002, pp. 1474–1572. http://www.fischer-tropsch.org/DOE/DOE_reports/40308/FC26-98FT40308-f/FC26-98FT40308-f_toc.htm (accessed 4 May, 2022).

[59] N.E. Tsakoumis, R. Dehghan-Niri, M. Rønning, J.C. Walmsley, Ø. Borg, E. Rytter, A. Holmen, X-ray absorption, X-ray diffraction and electronic microscopy study of spent cobalt-based catalyst in semi-commercial scale Fischer-Tropsch synthesis, Appl. Catal. A 479 (2014) 59–89.

[60] D. Krishnamurthy, A.M. Saib, D.J. Moodley, J.W. Niemantsverdriet, C. J. Weststrate, Ostwald ripening on a planar Co/SiO_2 catalyst exposed to model Fischer-Tropsch synthesis conditions, J. Catal. 328 (2015) 123–129.

[61] C.H. Mauldin, Cobalt catalysts for the conversion of methanol to hydrocarbons and for Fischer-Tropsch synthesis, United States patent 4,568,663, 1986.

[62] S. Eri, J. Goodwin, G. Marcelin, T. Riis, Catalyst for production of hydrocarbons, United States patent 4.801.573, 1987.

[63] C.H. Mauldin, D.E. Varnado, Rhenium as a promoter of titania-supported cobalt Fischer-Tropsch catalysts, Stud. Surf. Sci. Catal. 136 (2001) 417–422.

[64] A.-M. Hilmen, D. Schanke, A. Holmen, TPR study of the mechanism of rhenium promotion of alumina-supported cobalt Fischer-Tropsch catalysts, Catal. Lett. 38 (1986) 143–147.

[65] F. Diehl, A.Y. Khodakov, Promotion of cobalt Fischer-Tropsch catalysts with noble metals: a review, Oil Gas Sci. Technol.-Rev. IFP 64 (2009) 11–24.

[66] Ø. Borg, S. Eri, E.A. Blekkan, S. Storsæter, H. Wigum, E. Rytter, A. Holmen, Fischer-Tropsch synthesis over γ-alumina-supported cobalt catalysts: effect of support variables, J. Catal. 248 (2007) 89–100.

[67] Ø. Borg, N. Hammer, S. Eri, O.A. Lindvåg, R. Myrstad, E.A. Blekkan, M. Rønning, E. Rytter, A. Holmen, Fischer-Tropsch synthesis over un-promoted and Re-Promoted γ–Al_2O_3 supported cobalt catalysts with different pore sizes, Catal. Today 142 (2009) 70–77.

[68] C.G. Visconti, L. Lietti, E. Tronconi E, P. Forzatti, R. Zennaro, E. Finocchio, Fischer-Tropsch synthesis on a Co/Al_2O_3 catalyst with CO_2 containing syngas, Appl. Catal. A 355 (2009) 61–68.

[69] M. Hillestad, Modeling the Fischer–Tropsch product distribution and model implementation, Chem. Prod. Proc. Model. 10 (2015) 147–159.

[70] E. Rytter, A. Holmen, On the support in cobalt Fischer-Tropsch: emphasis on alumina and aluminates, Catal. Today 275 (2016) 11–19.

[71] G.L. Bezemer, J.H. Bitter, H.P.C.E. Kuipers, H. Oosterbeek, J.E. Holewijn, X- Xu, F. Kapteijn, A.J. van Dillen, K.P. de Jong, Cobalt particle size effects in the Fischer-Tropsch reaction studied with carbon nanofiber supported catalysts, J. Am. Chem. Soc. 128 (2006) 3956–3964.

[72] Ø. Borg, P.D.C. Dietzel, A.I. Spjelkavik, E.Z. Tveten, J.C. Walmsley, S. Diplas, S. Eri, A. Holmen, E. Rytter, Fischer-Tropsch synthesis: cobalt particle size and support effects on intrinsic activity and product distribution, J. Catal. 259 (2008) 161–164.